Terahertz circular dichroism of R/S-MBA_2PbI_4

Sierra Whipple

A senior thesis submitted to the faculty of
Brigham Young University
in partial fulfillment of the requirements for the degree of

Bachelor of Science

Dr. John Colton, Advisor

Department of Physics and Astronomy

Brigham Young University

ABSTRACT

Terahertz circular dichroism of R/S-MBA_2PbI_4

Sierra Whipple
Department of Physics and Astronomy, BYU
Bachelor of Science

R/S-MBA_2PbI_4 is a metal halide perovskite composed of chiral organic layers and non-chiral inorganic layers. The organic layers can impart some of their chiral properties to the inorganic layers, causing the material overall to exhibit circular dichroism. We developed a model to determine the terahertz circular dichroism (TCD) of our material using a traditional terahertz time domain spectroscopy setup (THz-TDS). The TCD is determined using a series of model fits. The project is ongoing, but preliminary data gives evidence that R/S-MBA_2PbI_4 exhibits non-negligible TCD.

Keywords: [terahertz time domain spectroscopy, terahertz circular dichroism, metal halide perovskites, chirality]

ACKNOWLEDGMENTS

Great thanks to Dr. John Colton of Brigham Young University for providing me the opportunity to assist with this project and for guiding me through every step of the process. Thanks to our collaborators at the National Renewable Energy Laboratory, Matt Beard and Yifan Dong. Thanks to my parents, Chris and Briana Williams, and my husband, Adam, for being a constant source of encouragement and confidence. Thanks to the Physics Department at Brigham Young University and generous donors who provide funding for my participation in research.

Contents

Chapter 1

Motivation and Theory

1.1 Chiral Phonons

A phonon is a fundamental excitation in condensed matter physics [1]. A phonon can be described as the quantum of energy caused by a collective excitation in an arrangement of atoms or molecules in condensed matter, in our case this condensed matter is the solid metal halide perovskite [2]. Traditionally phonons are considered to be linearly polarized and non-chiral (see sec. 1.2 for more about chirality). However, recent studies show that there are phonons of special oscillation modes with circular polarization and angular momentum. These have been named chiral phonons [1]. Chiral phonons play an important role in many physical properties of condensed matter systems, including spintronics, 2D optoelectronics, and thermodynamics [3].

Chiral phonons can be useful in generating and detecting circularly polarized light. This could be utilized in quantum computing and quantum communications. We are interested in studying the chiral properties of metal halide perovskites to determine their potential for use in such applications.

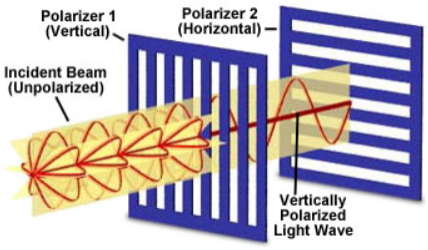

Figure 1.1 Linear Polarization of Light. Unpolarized light passes through a vertical polarizer. The resulting vertically polarized light passes through a horizontal polarizer and none is transmitted. From Ref. [4].

1.2 Chirality and Circular Dichroism

In general, electromagnetic waves can oscillate in an infinite number of planes perpendicular to the direction of propagation. To examine the properties of light effectively, we may choose one plane of oscillation and filter out any fraction of the light that is not oscillating in the plane. Light that is restricted to a single plane of oscillation is called linearly polarized light. This concept is illustrated in Fig. 1.1 [4].

Light can also be circularly polarized. This occurs when light is composed of two orthogonal plane waves traveling out of phase with each other by 90 degrees. Linearly polarized light can be described as the superposition of left circularly polarized light (LCP) and right circularly polarized light (RCP), whose phase difference will determine the angle θ of the linearly polarized superposition [5].

When linearly polarized light passes through a chiral material, the plane of polarization is rotated. This happens due to a phenomenon called "circular birefringence." In a chiral material, the index of refraction is different for left and right circularly polarized light. Therefore, left and right circularly polarized light will travel at different speeds through a chiral material, introducing a new phase shift between the two. As the phase shift between the two circular polarizations changes, the angle of linear polarization, θ, will also change.

In addition to circular birefringence, linearly polarized light is affected by circular dichroism (CD), which is the difference in absorption in right and left circularly polarized light. Both CD and circular birefringence are used to describe how the polarization of light is affected as it passes through a material. Many techniques exist to determine the circular dichroism of a material, but each method is specific to a particular range of energies. For example, one method to measure electronic circular dichroism, ECD, works well with changes in ultraviolet or visible light [6]. Another method, using vibrational circular dichroism (VCD) is best for near- and mid-infrared energies [6]. Terahertz circular dichroism (TCD) is circular dichroism determined by frequencies on the range of terahertz rather than in the optical or visible light range. TCD spectroscopy is less developed than other optical techniques, but like VCD, it detects vibrations. Unlike VCD, TCD detects vibrations in the terahertz range. The typical vibrational frequency for solids is 10^{13} Hz [7], which makes TCD so useful, as it can detect much higher frequencies.[1] For this reason, TCD is highly sensitive to three-dimensional structures in solids, providing a way to characterize chiral phonons and other phenomena [6].

TCD is most often reported in units of molar ellipticity, θ in Fig. 1.2, though it can also be reported in units of absorbance. Data from many CD instruments will be reported directly in units of absorbance, which is often transformed to molar ellipticity. Molar ellipticity is preferred as it corrects the CD for concentration of the sample (a longer, more dense sample will have a greater effect on the light than a small sample). Molar ellipticity is proportional to CD, using the sample concentration, cell pathlength, and molecular weight as conversion factors [8]. In our experiment, which does not use CD instrumentation, TCD can be determined by calculating the molar ellipticity, or determining the amplitudes of the left and right circularly polarized fields (E_L and E_R). Using molar ellipticity, we can say that TCD is proportional to the inverse tangent of the angle between

[1] THz light is 10^{12} Hz.

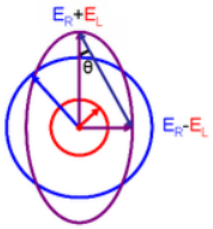

Figure 1.2 Molar Ellipticity. The blue line represents the right circularly polarized field, $\mathbf{E}_R$. The red represents the left circularly polarized field, $\mathbf{E}_L$. The purple line represents total electric field. θ is the angle between the maximum electric field and minimum electric field. From Ref. [9].

the normalized difference of the left and right circularly polarized (LCP and RCP) electric field (see Fig. 1.2 and Eq. 1.1) [5].

$$\tan(\theta) = \frac{E_R - E_L}{E_R + E_L} \tag{1.1}$$

Chiral molecules have special orientation in space and are considered to be "optically active", meaning that an electric field is rotated as it passes through the material. In other words, chiral molecules exhibit circular dichroism. Chiral molecules come in pairs, or enantiomers, designated with an R- or S- prefix. These enantiomers typically rotate light by approximately the same amount in different directions. For example, the R-enantiomer will rotate the electric field clockwise, while the S-enantiomer will rotate the electric field counterclockwise. In our experiment, for light of a given wavelength, we expect to to see relatively equal amounts of polarization rotation in opposite directions when comparing the R- and S- enantiomers.

1.3 Jones and Mueller Matrices

Jones calculus is used to describe the polarization state of light. Jones calculus uses a 2×1 Jones vector to describe the polarization state of light and a 2×2 Jones matrix to describe transformations of light. We will use Jones calculus to describe the effects of our sample on the signal. The most relevant Jones matrices have been defined and we will reference them throughout our paper. These matrices represent **V**: a vertical polarizer, **H**: a horizontal polarizer, **P**: a linear polarizer at an angle θ, and **M**: a material Jones matrix. Equations 1.2, 1.3. and 1.4 describe the Jones matrices for a vertical, horizontal, and general linear polarizer at an angle θ, respectively.

$$\mathbf{V} = \begin{bmatrix} 0 & 0 \\ 0 & 1 \end{bmatrix} \tag{1.2}$$

$$\mathbf{H} = \begin{bmatrix} 1 & 0 \\ 0 & 0 \end{bmatrix} \tag{1.3}$$

$$\mathbf{P} = \begin{bmatrix} \cos^2\theta & \cos\theta\sin\theta \\ \cos\theta\sin\theta & \sin^2\theta \end{bmatrix} \tag{1.4}$$

The material Jones matrix for our sample is written as [2]:

$$\mathbf{M} = \begin{bmatrix} t_{xx} & t_{xy} \\ t_{yx} & t_{yy} \end{bmatrix} \tag{1.5}$$

Additionally, the Jones matrix for a sample rotated by 90 degrees is $M_{rot} = R \cdot M \cdot R^{-1}$, where R is the standard rotation matrix with θ = 90: $\left[\begin{smallmatrix} \cos\theta & -\sin\theta \\ \sin\theta & \cos\theta \end{smallmatrix}\right]$. Therefore, the Jones matrix for a sample rotated by 90 degrees is M_{rot}, as shown in Eq. 1.6.

[2] We will use the convention outlined in Eq. 1.6. This convention differs from that used by Cheng et al [10]

$$\mathbf{M_{rot}} = \begin{bmatrix} t_{yy} & -t_{yx} \\ -t_{xy} & t_{xx} \end{bmatrix} \tag{1.6}$$

The elements of the Jones matrix for a material can be experimentally determined and describe how the material transforms light that passes through it. In our case, the matrix helps us calculate the terahertz circular dichroism (TCD), which relates to the elements of the material Jones matrix. This will be described in more detail in Section 3.3.

1.4 Metal-Halide Perovskites

Halide perovskites are a specific type of perovskite, where a perovskite is any material with a crystal structure following the formula ABX_3, as shown in Fig. 1.3. A and B are two positively charged cations, while X is a negatively charged anion [11]. Halide perovskites specifically include halides (Cl, Br, or I) as the X ion and therefore are semiconductors with special properties [12]. The perovskites we are most interested in use organic cations in place of the A ion. If the organic molecules are large enough, the metal halide regions separate into 2d layers, changing the formula ABX_3 to A_2BX_4. In our example, R/S-MBA_2PbI_4 uses methyl-benzyl-ammonium (MBA) for A, lead (Pb) for B, and iodine (I) for X.

Metal halide perovskites are being found to be very promising materials. One study by Lu, Vardeny, and Beard, suggests that chiral halide perovskites can be useful in the control of light, spin and charge without magnetic components [13]. However, in other materials a magnetic field is typically necessary to control the spin of the electrons while electric fields control the movement of the charges. Because semiconductors are non-magnetic systems that allow for charge transport and absorption or emission of light, being able to control the spin at the spin of the charges as they move without a magnetic field would be incredibly beneficial. Chiral molecules can control the spin

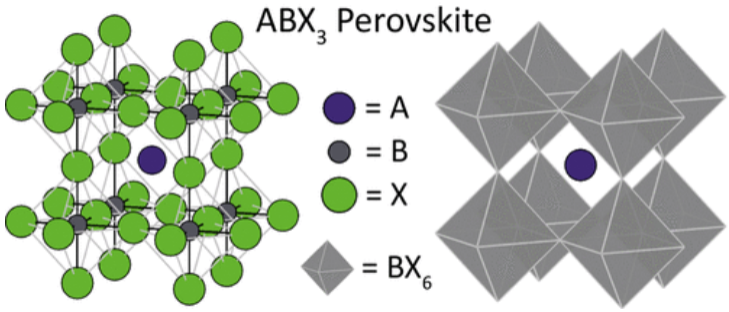

Figure 1.3 Standard depiction of an ABX_3 perovskite. The left shows each individual atom. The right shows the A atom and the BX_6 octahedral network. From Ref. [12].

of an electron without a magnetic field and act as a spin filter, letting only electrons of a specific spin (spin up or spin down) enter the material. Therefore, inducing chirality in a semiconductor will allow for control of spin during transport of charges [13]. Therefore, we will attempt to analyze chiral properties of the metal halide perovksite, R/S-MBA_2PbI_4.

Chapter 2

Methods

2.1 Current Literature

Gong Cheng, et. al. published a paper describing techniques to characterize chiral and anisotropic (directionally-dependent) materials using terahertz time-domain polarimetry (THz-TDP), using a basic terahertz time-domain spectrometry (THz-TDS) setup with the addition of three linear polarizers. We use this paper as a guideline for our experiment (see Section 2.2). The setup begins with a THz emitter, oriented vertically. The light passes through a vertical polarizer (P1), to ensure that the light is polarized along the vertical direction before being focused onto the sample. After passing through the sample, the light passes through a rotatable polarizer, P2. Finally, the light passes through P3, oriented horizontally (90 degrees relative to P1) to further increase the sensitivity and is detected by a THz detector oriented horizontally (see Fig. 2.1) [10].[1]

In the paper, the authors suggest that the total electric field after the sample and its corresponding polarization can be determined by only three measurements. The measurements include setting the

[1] In reality, the Cheng et al paper orients P1 horizontally and P3 vertically (opposite of the setup in our experiment). For consistency throughout this thesis, we use the orientation consistent with our experiment, and all calculations reflect this designation [10].

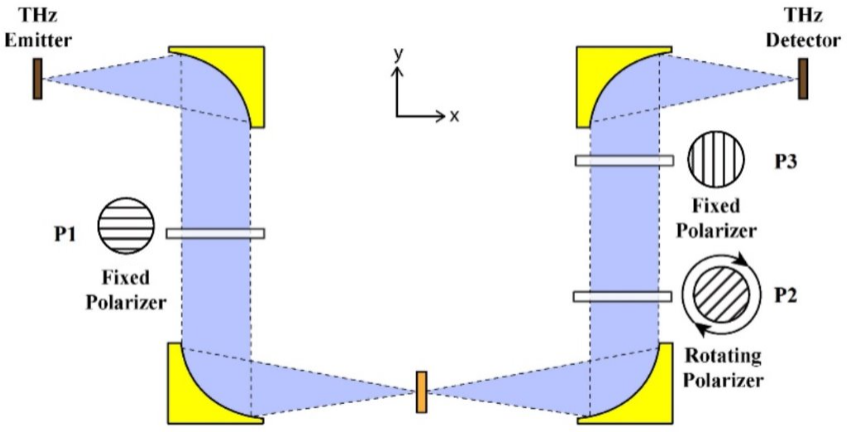

Figure 2.1 Schematic illustration of THz spectrometer at NREL. The THz emitter is oriented such that the polarization of the generated THz pulse is vertical, and the direction of the THz detector is horizontal. P1 is a vertical polarizer. P2 is a rotatable polarizer. P3 is a horizontal polarizer. The Cheng et al paper uses an opposite setup, swapping P1 and P3. Figure adapted from Ref. [10].

rotatable polarizer, P2, to 0 degrees, +45 degrees, and -45 degrees (relative to P3). The horizontal component of the electric field just after passing through the sample, E_x, is simply determined when P2 is set to 0 degrees (aligned with P3). The vertical component of the field just after passing through the sample, E_y, is determined by subtracting the results with the rotatable polarizer, P2, set to +45 and -45 degrees, denoted E_{+45} and E_{-45}, respectively. To prove this, say that the field before P2 is $\begin{bmatrix} E_x \\ E_y \end{bmatrix}$, then after P2, at an angle θ, and the horizontal polarizer, P3, the resulting field can be described by Eq. 2.1.

$$\begin{bmatrix} det_x \\ det_y \end{bmatrix} = \begin{bmatrix} 1 & 0 \\ 0 & 0 \end{bmatrix} \cdot \begin{bmatrix} \cos^2\theta & \cos\theta\sin\theta \\ \cos\theta\sin\theta & \sin^2\theta \end{bmatrix} \begin{bmatrix} E_x \\ E_y \end{bmatrix} \tag{2.1}$$

Matrix multiplication of Eq. 2.1 gives $det_x = \sin(\theta)\cos(\theta)\cdot E_y + \cos^2(\theta)\cdot E_x$. The E_{+45} and E_{-45} measurements are det_x with θ = +45 and -45. respectively. Therefore, we prove that $E_y = E_{+45}$ - E_{-45}.

$$E_y = E_{+45} - E_{-45} \tag{2.2}$$

$$E_y = \sin(45)\cdot\cos(45)\cdot E_y + \cos^2(45)\cdot E_x - (\sin(-45)\cdot\cos(-45)\cdot E_y + \cos^2(-45)\cdot E_x) \tag{2.3}$$

$$\sin(-x) = -\sin(x) \tag{2.4}$$

$$\cos(-x) = \cos(x) \tag{2.5}$$

$$E_y = \sin(45)\cdot\cos(45)\cdot E_y + \cos^2(45)\cdot E_x - (-\sin(45)\cdot\cos(45)\cdot E_y + \cos^2(45)\cdot E_x) \tag{2.6}$$

$$E_y = 2\cdot\sin(45)\cdot\cos(45)\cdot E_y \tag{2.7}$$

$$E_y = 2\cdot\frac{1}{\sqrt{2}}\cdot\frac{1}{\sqrt{2}} \tag{2.8}$$

$$E_y = E_y \tag{2.9}$$

A fast Fourier transform is performed on these time-domain signals for E_x and E_y to obtain the frequency-domain spectra. The resulting frequency-domain data is used for all further calculations. In this section, I will give the definitions from the Cheng et al paper, using the geometry of our experiment. Later, I will give the definitions and equations used in our calculations, which have some modifications (see Sections 3.1-3.3).

The frequency-dependent Jones matrix determines the optical properties of the sample, including chirality. Assume the THz light emitted has a Jones vector $\begin{bmatrix} 0 \\ E_{ref} \end{bmatrix}$ and define the light after the sample (before P2) as $\begin{bmatrix} E_{sx}^{(1)} \\ E_{sy}^{(1)} \end{bmatrix}$.[2] Therefore, the electric field before and after the sample are related by Eq. 2.10. [3]

$$\begin{bmatrix} E_{sx}^{(1)} \\ E_{sy}^{(1)} \end{bmatrix} = \begin{bmatrix} t_{xx} & t_{xy} \\ t_{yx} & t_{yy} \end{bmatrix} \begin{bmatrix} 0 \\ E_{ref} \end{bmatrix} \tag{2.10}$$

[2]The (1) superscript in each element denotes the initial orientation of the sample.

[3]Cheng et al use a different notation for the Jones matrix. That is, t_{xy} and t_{yx} are reversed. For consistency, here I use the notation we used for the NREL calculations.

Therefore, two coefficients of the material Jones matrix can be determined by solving the matrix equation for t_{xy} and t_{yy} (Eq. 2.11), resulting in Eqs. 2.12 and 2.13.

$$\begin{aligned} E_{sx}^{(1)} &= t_{xy} \cdot E_{ref} \\ E_{sy}^{(1)} &= t_{yy} \cdot E_{ref} \end{aligned} \tag{2.11}$$

$$t_{xy} = E_{sx}^{(1)} / E_{ref} \tag{2.12}$$

$$t_{yy} = E_{sy}^{(1)} / E_{ref} \tag{2.13}$$

To determine the remaining coefficients. t_{xx} and t_{yx}, rotate the sample by 90 degrees and designate the Jones vector for the light after passing through the rotated sample $\begin{bmatrix} E_{sx}^{(2)} \\ E_{sy}^{(2)} \end{bmatrix}$.[4] The material Jones matrix for a sample rotated by 90 degrees is $\begin{bmatrix} t_{yy} & -t_{yx} \\ -t_{xy} & t_{xx} \end{bmatrix}$ (see Section 1.3).

Then, applying the same process as before with the electric field before and after the rotated sample, we find Eq. 2.14.

$$\begin{bmatrix} E_{sx}^{(2)} \\ E_{sy}^{(2)} \end{bmatrix} = \begin{bmatrix} t_{yy} & -t_{yx} \\ -t_{xy} & t_{xx} \end{bmatrix} \begin{bmatrix} 0 \\ E_{ref} \end{bmatrix} \tag{2.14}$$

Performing matrix multiplication on Eq. 2.14 yields Eq. 2.15. Solving Eq. 2.15 for t_{xx} and t_{yx} gives Eqs. 2.16 and 2.17.

$$\begin{aligned} E_{sx}^{(2)} &= -t_{yx} \cdot E_{ref} \\ E_{sy}^{(2)} &= t_{xx} \cdot E_{ref} \end{aligned} \tag{2.15}$$

$$t_{yx} = -E_{sx}^{(2)} / E_{ref} \tag{2.16}$$

[4]The (2) superscript in each element denotes the second orientation of the sample (after rotating by 90 degrees.)

$$t_{xx} = E_{sy}^{(2)} / E_{ref} \tag{2.17}$$

If the sample is isotropic (not directionally dependent) then $E_{sx}^{(1)} = E_{sx}^{(2)}$ and $E_{sy}^{(1)} = E_{sy}^{(2)}$ because rotating the sample has no effect on the light passing through. Therefore, $t_{xx} = t_{yy}$ and $t_{xy} = -t_{yx}$.

With the coefficients of the material Jones matrix calculated, the TCD can be calculated by examining the magnitude of the electric field vectors for RCP and LCP light that would pass through the material, as discussed in Sec 1.2.

$$TCD = \tan^{-1}\left(\frac{E_R - E_L}{E_R + E_L}\right) \tag{2.18}$$

E_R and E_L are the magnitudes of the right and left circularly polarized electric field vectors, respectively. To derive the equations for E_R and E_L, begin with the complex vectors describing the right and left circularly polarized fields. For RCP and LCP, the electric field is described by $\mathbf{E}_{in}^{RCP} = \frac{1}{\sqrt{2}}\begin{bmatrix}1\\-i\end{bmatrix}$ and $\mathbf{E}_{in}^{LCP} = \frac{1}{\sqrt{2}}\begin{bmatrix}1\\i\end{bmatrix}$.[5] Then, to describe LCP and RCP portions of the light after it has passed through the sample, perform the following operations (Eqs. 2.19 and 2.20).

$$\mathbf{E}_s^{RCP} = \mathbf{T}\cdot\mathbf{E}_{in}^{RCP} = \begin{bmatrix}t_{xx} & t_{xy}\\ t_{yx} & t_{yy}\end{bmatrix}\frac{1}{\sqrt{2}}\begin{bmatrix}1\\-i\end{bmatrix} = \frac{1}{\sqrt{2}}\begin{bmatrix}t_{xx}-it_{xy}\\ t_{yx}-it_{yy}\end{bmatrix} \tag{2.19}$$

$$\mathbf{E}_s^{LCP} = \mathbf{T}\cdot\mathbf{E}_{in}^{LCP} = \begin{bmatrix}t_{xx} & t_{xy}\\ t_{yx} & t_{yy}\end{bmatrix}\frac{1}{\sqrt{2}}\begin{bmatrix}1\\i\end{bmatrix} = \frac{1}{\sqrt{2}}\begin{bmatrix}t_{xx}+it_{xy}\\ t_{yx}+it_{yy}\end{bmatrix} \tag{2.20}$$

Then E_R and E_L are defined to be the magnitudes of the complex vectors $\mathbf{E}_s^{RCP}$ and $\mathbf{E}_s^{LCP}$ respectively as shown in Eqs. 2.21 and 2.22.

$$E_R = \sqrt{\left(\frac{\left|(t_{xx}-it_{xy})\right|^2 + \left|(t_{yx}-it_{yy})\right|^2}{2}\right)} \tag{2.21}$$

[5] Here again, the Cheng paper uses a different convention to describe RCP and LCP. For consistency, I will report these equations using the convention we used for the NREL data analysis.

$$E_L = \sqrt{\left(\frac{\left|(t_{xx} + it_{xy})\right|^2 + \left|(t_{yx} + it_{yy})\right|^2}{2}\right)} \tag{2.22}$$

2.2 NREL Experiment

John Colton, Yifan Dong, and Matt Beard conducted an experiment at the National Renewable Energy Lab (NREL) in Colorado. The purpose of this experiment was to measure the circular dichroism of the R/S-MBA_2PbI_4 as it manifests itself on the rotation of linearly polarized incident light. R/S-MBA_2PbI_4, methyl-benzyl-ammonium lead iodide, is a metal halide perovskite with chiral properties. The interaction between the chiral organic molecules and the inorganic framework is suspected to cause chirality transfer, giving the inorganic layers in the perovskite chiral properties [14].

In this experiment, terahertz light was produced via a cadmium telluride (CdTe) crystal. The emitted light is polarized along the vertical axis. The light then passes through an initial polarizer, P1, which is designated as the vertical axis, ensuring that the light was truly vertical. Then the light passes through a sample or reference material. If the sample has chiral properties, the polarization of the light will be rotated. Next, the light passes through a rotatable polarizer, and finally through a horizontal polarizer, P3, before hitting a detector specifically sensitive to terahertz light oriented along the horizontal axis (see Fig. 2.1).

The largest differences between the Cheng et al experimental setup and NREL are the assumptions made. At NREL, rather than use only three angles for the rotatable polarizer, P2, we use multiple angles and perform a model fit to calculate E_x and E_y (see Sections B and 3.2). Additionally, we do not assume that our reference light (the light before the sample) is perfectly linearly polarized along the vertical axis. Although the Cheng et al paper assumes P1 and P3 are orthogonal, we consider the case that they are not. If P1 and P3 are not orthogonal, the reference light in the

horizontal light would be small, but non-zero. We find that the horizontal component needs to be small but non-zero to obtain good fits for the data (see Section 3.2).

For the typical NREL experiments, we examine two samples: pure R-MBA_2PbI_4 and pure S-MBA_2PbI_4, each deposited onto a substrate. We also take reference data on the substrate alone and air (no sample or substrate). Each sample is made by depositing R/S-MBA_2PbI_4 on a quartz or sapphire substrate. To test our setup, we expect to observe approximately equal amounts of rotation in opposite directions in the R- and S- samples.

This experiment is ongoing. As of June 2024, three groups of data have been collected. On September 27th, 2023, data was collected on only one sample: 5 layers of R-MBA_2PbI_4 on sapphire. Each data set was taken over a period of 11.2 picoseconds (ps) labeled from -3.2 ps to 8 ps in intervals of 0.1 ps. This was done for 13 angles, ranging from 90 degrees to 90 degrees in 15-degree intervals.[6]

On October 19th, 2023, data was collected on two samples: one each of R- and S-MBA_2PbI_4 on quartz (both only one layer of substrate). Each data set was taken over a period of 15 ps (-5 ps to 10 ps) in intervals of 0.1 ps. This was done for 9 angles, ranging from -60 degrees to 60 degrees in 15-degree intervals.

On May 31st, data was collected on two samples, one each of R- and S-MBA_2PbI_4 on sapphire (each 5 layers of sample on substrate).[7] Each data set was taken over a period of 11.2 ps (-3.2 to 8 ps in intervals of 0.1 ps.)[8]

[6]File Sep27_002, the air data includes 26 angles form 90 degrees to 35 degrees in 5-degree increments.

[7]Multiple stacks increases the path length of the sample, providing the opportunity for larger TCD signals.

[8]File May30_002 contains air data with time intervals of 0.8 ps. Normally, the same separation is necessary to perform the calculations described in sec 3.3. In this case, adjustments were made to extrapolate data.

Chapter 3

Data Analysis

At the conclusion of data collection, for each sample and reference, we have a set of electric field data versus time for each angle.[1] This is done by producing terahertz light and measuring the electric field over a period of time with the rotatable polarizer set to a different angle each time (P2 in Fig. 2.1). First, we use the reference data sets to calculate the error in our rotatable polarizer, P2. With this information, we can calculate the horizontal and vertical components of the electric field (after the sample, before P2), E_x and E_y, accounting for the error in P2 and the error between P1 and P3. Finally, we use the magnitudes of $\mathbf{E}_R$ and $\mathbf{E}_L$ to calculate the TCD of R/S-MBA_2PbI_4.

Figs. 3.1 and 3.2 are examples of the raw data for two specific polarizer angles. For each sample, we take a set of time data at various angles of P2, typically from -90 to 90 degrees in intervals of 5-15 degrees. More angles will give us a more accurate model fit when calculating error in P2 and the field magnitude after the sample.

[1] Recall that rather than the three angles, -45, 0, and 45 degrees, we use a wide array of angles for P2.

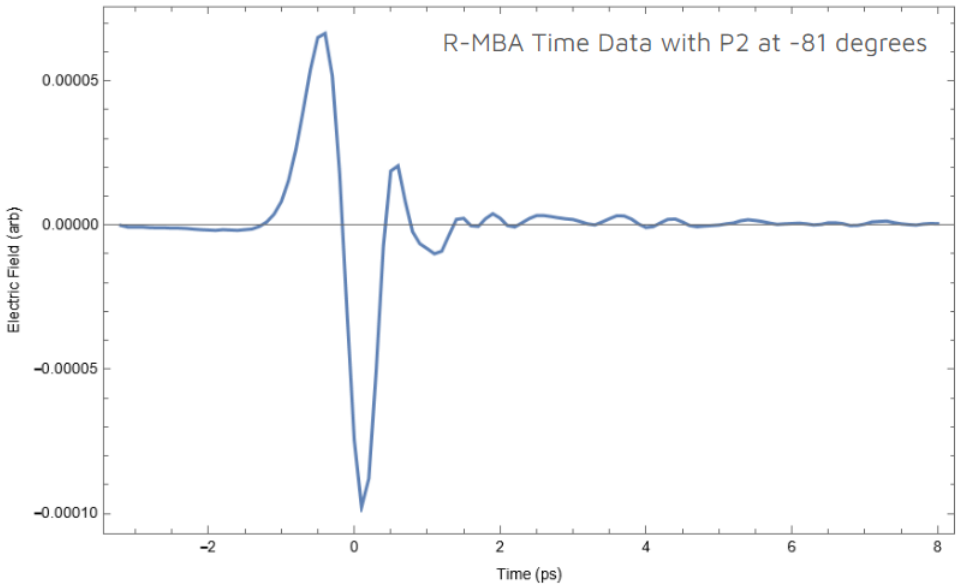

Figure 3.1 Example of Raw Data. Sample is R-MBA_2PbI_4. Data taken on May 31, 2024. Time of -3.2 to 8 ps in time steps of 0.1 p.s. P2 is set to -81 degrees (relative to horizontal).

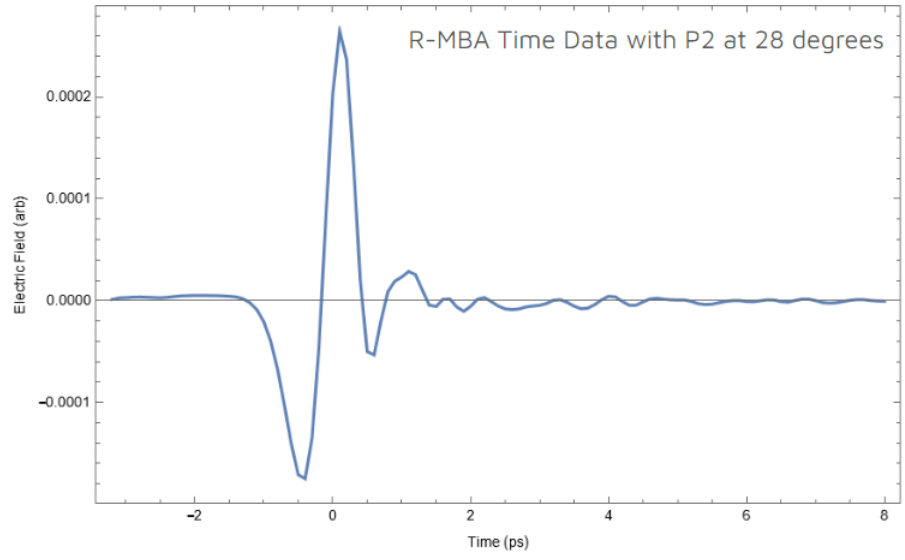

Figure 3.2 Example of Raw Data. Sample is R-MBA_2PbI_4. Data taken on May 31, 2024. Time of -3.2 to 8 ps in time steps of 0.1 p.s. P2 is set to 28 degrees (relative to horizontal).

3.1 Calculation of Offset in Rotatable Polarizer

In the early days of this experiment at NREL, the rotatable polarizer P2 was removed from its mount and stored in a case overnight each day. When the polarizer is mounted each morning, it is done by hand. It is very difficult to align the polarizer perfectly when it is mounted. Therefore, we cannot assume that the angle of the rotatable polarizer is the same angle that is recorded in the data. It could be off by anywhere from 0 to 180 degrees. For this purpose, we must fit the reference data to a model to define the offset of the rotatable polarizer. This offset will be the same for each date that data is taken as once the polarizer is mounted the angle is rotated automatically and the error is consistent throughout the day. Therefore, we only need to calculate the initial error when the polarizer is mounted.

Recall Fig. 2.1 where we define P1 to be vertical, P2 is a variable angle (theta relative to horizontal), and P3 is horizontal. With no sample in place, when P2 is set to 0 or 90 degrees (relative to the horizontal axis), no light gets through P3. If P2 is at an intermediate angle theta, then after P2 the electric field is reduced to $\cos(\theta)$ of the original field and it is polarized at the angle θ (see Fig. 3.3). After P3 there is another reduction in field amplitude, by a factor of $\cos(90^\circ - \theta) = \sin(\theta)$ (see Fig. 3.4), so the final amplitude is $\sin(\theta)\cos(\theta) = \frac{1}{2}\sin(2\theta)$. The intensity therefore should vary as a function of angle according to $\sin^2(2\theta)$. This is true for each frequency component, as well as for the wave overall.

Using this relationship, any error in the angle of P2 can be calculated using the reference data taken in the experiment. Take the equation derived in the previous paragraph: $det = \frac{1}{2}\sin(2\theta)$, where det is the measured field amplitude. First, call $\theta = x - x_0$, where x_0 is the error in the rotatable polarizer, P2. Then, for each time point, fit the data (amplitude vs angle) to the following model:

$$det = A_i \sin(2(x - x_0)) \tag{3.1}$$

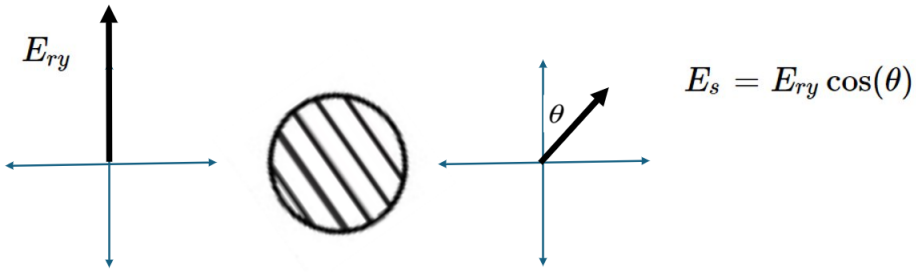

Figure 3.3 Field Magnitude after P2

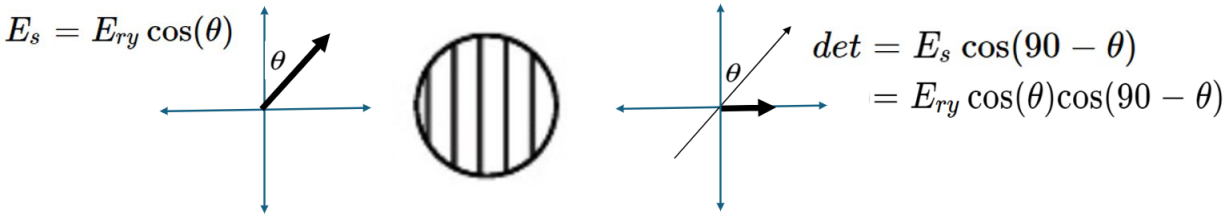

Figure 3.4 Field Magnitude after P3

where the magnitude of the signal, A_i, varies depending on the frequency of the oscillations. The magnitude of each signal will vary with frequency, but the angle offset will be the same for each data set. Because we have multiple data sets with a shared parameter (x_0), we can perform a special model fit called a MultiNonlinearModelFit, with documentation in Mathematica (see Appendix A). The MultiNonlinearModelFit takes multiple data sets with at least one shared parameter and fits them to the same model. Fig. 3.5 shows an example of the MultiNonLinearModelFit results. After rearranging the data by time point in sets of amplitude versus angle, the model fit is applied to determine the offset of P2 from the assumed angle.

In this case, the shared parameter x_0 is of particular interest. This value can be subtracted from the recorded angles of subsequent data sets to give obtain a more accurate calculation of E_x and E_y data. For example, the reference data taken on October 19th (File Oct19_002.tim) yielded a minus 23 degree offset. Therefore, in subsequent data sets taken on that same day (R-MBA_2PbI_4 and

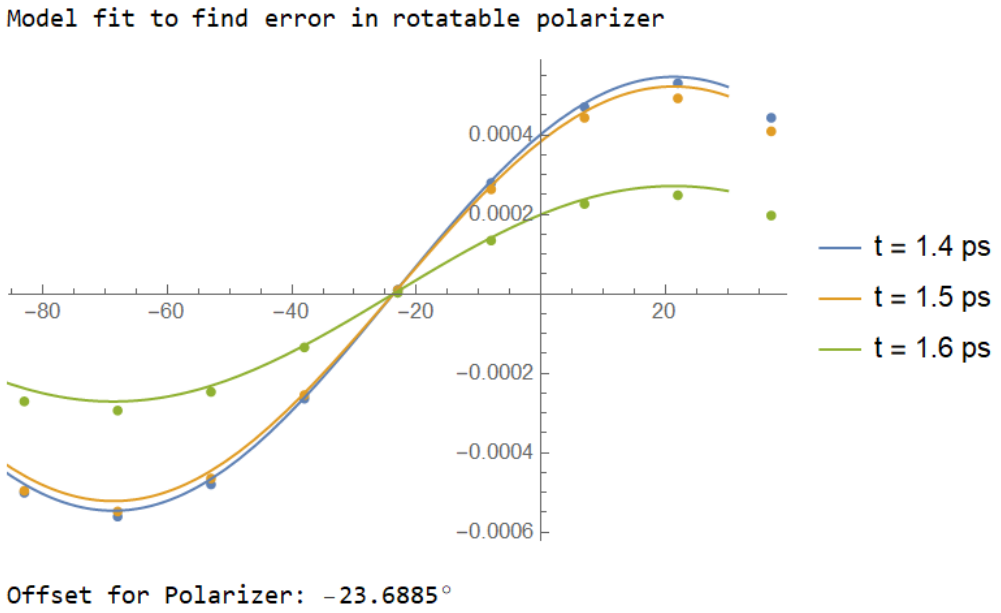

Figure 3.5 Angle Offset Fit Results October 19. This is an example of the angle fit for three time points. Note that each have the same x-intercept, x_0, around -23 degrees.

S-MBA_2PbI_4), before any calculations are performed, -23 degrees is subtracted from each angle in the angle list.

Appendix B shows the Mathematica code used to calculate the offset in the rotatable polarizer.

3.2 Calculation of E_x and E_y

The first step to calculate TCD is to determine the horizontal and vertical components of the electrical field after the light has passed through the sample (between the sample and P2 in Fig. 2.1).

The Jones vector for the light after passing through the sample can be written as $\begin{bmatrix} E_x \\ E_y \end{bmatrix}$, where E_x is the horizontal component of the field amplitude and E_y is the vertical component. This light will pass through P2, the rotatable polarizer. The Jones Matrix for P2 is $\begin{bmatrix} \cos^2(\theta) & \cos(\theta)\sin(\theta) \\ \cos(\theta)\sin(\theta) & \sin^2(\theta) \end{bmatrix}$, where θ is the angle of P2 adjusted by the offset calculated previously (see Section 3.1). Finally, the light

passes through P3, the horizontal polarizer, before being received at the detector. The Jones matrix for a horizontal polarizer is simply $\left[\begin{smallmatrix}1 & 0\\ 0 & 0\end{smallmatrix}\right]$.

Overall, the matrix equation for this light is represented by Eq. 3.2 (see Section 1.3).

$$\begin{bmatrix} det_x \\ det_y \end{bmatrix} = \begin{bmatrix} 1 & 0 \\ 0 & 0 \end{bmatrix} \begin{bmatrix} \cos^2(\theta) & \cos(\theta)\sin(\theta) \\ \cos(\theta)\sin(\theta) & \sin^2(\theta) \end{bmatrix} \begin{bmatrix} E_x \\ E_y \end{bmatrix} \tag{3.2}$$

Performing matrix multiplication on this equation yields Eq. 3.3.

$$\begin{bmatrix} det_x \\ det_y \end{bmatrix} = \begin{bmatrix} 1 & 0 \\ 0 & 0 \end{bmatrix} \begin{bmatrix} \cos^2(\theta)E_x + \cos(\theta)\sin(\theta)E_y \\ \cos(\theta)\sin(\theta)E_x + \sin^2(\theta)E_y \end{bmatrix} \tag{3.3}$$

After passing through the horizontal polarizer, the vertical component, det_y is equal to zero. Therefore, the total measured signal is equal to det_x, represented below, according to Eq. 3.4. We will use Eq. 3.4 to fit our data and find a value for E_x and E_y.

$$det_x = \sin(\theta)\cos(\theta)\cdot E_y + \cos^2(\theta)\cdot E_x \tag{3.4}$$

With Eq. 3.4 as a model, we fit each set of intensity versus angle data to find the best-fit parameters E_x and E_y. We do this for each time point and store the values in an array. In the end, we have intensity versus time data for E_x and E_y. We plot these to confirm trends, shown in figs. 3.6 and 3.7.

Now that the E_x and E_y values have been calculated for each time point, we perform a fast Fourier transform on each data set (E_x in time and E_y in time) to find the value of the field (in terms of horizontal and vertical components) at each frequency. This brings us one step closer to calculating the TCD for each frequency. Figs. 3.8 and 3.9 show examples of the data in Figs. 3.6 and 3.7 after performing the Fourier transform. Appendix C shows the Mathematica code used to calculate E_x and E_y.

3.3 Calculation of TCD

The next step to calculate the TCD of our sample is to obtain the Jones matrix for the sample. The Jones Matrix shows what will happen to light as it passes through the material. For example, light polarized some amount, "E_{xr}", horizontally, and "E_{yr}" vertically, will be transformed by the Jones matrix, resulting in a different polarization, "$E_{xs}^{(1)}$" and "$E_{ys}^{(1)}$", as shown below. [3] [4]

$$\begin{bmatrix} E_{xs}^{(1)} \\ E_{ys}^{(1)} \end{bmatrix} = \begin{bmatrix} t_{xx} & t_{xy} \\ t_{yx} & t_{yy} \end{bmatrix} \begin{bmatrix} E_{xr} \\ E_{yr} \end{bmatrix} \tag{3.5}$$

Additionally, for a sample rotated by 90 degrees, the matrix equation is as shown:[5]

$$\begin{bmatrix} E_{xs}^{(2)} \\ E_{ys}^{(2)} \end{bmatrix} = \begin{bmatrix} t_{yy} & -t_{yx} \\ -t_{xy} & t_{xx} \end{bmatrix} \begin{bmatrix} E_{xr} \\ E_{yr} \end{bmatrix} \tag{3.6}$$

This yields the following equations for the field after passing through the sample, E_{xs} and E_{ys}, in terms of Jones Matrix components and the reference data of the field, E_{xr} and E_{yr}.

$$E_{xs} = t_{xx} \cdot E_{xr} + t_{xy} \cdot E_{yr} \tag{3.7}$$

$$E_{ys} = t_{yx} \cdot E_{xr} + t_{yy} \cdot E_{yr} \tag{3.8}$$

$$E_{xs} = t_{yy} \cdot E_{xr} - t_{yx} \cdot E_{yr} \tag{3.9}$$

$$E_{ys} = -t_{xy} \cdot E_{xr} + t_{xx} \cdot E_{yr} \tag{3.10}$$

[3] The subscript 'r' refers to the reference data (light before passing through the sample) and the subscript 's' refers to the 'sample' data or the magnitude of the field after passing through the sample, before any polarizers.

[4] The (1) superscript in each element denotes the initial orientation of the sample.

[5] The (2) superscript in each element denotes the second orientation of the sample (after being rotated by 90 degrees.)

Solving these Eqs. 3.7-3.10 for t_{xx}, t_{xy}, t_{yx}, and t_{yy} in terms of E_{xr}, E_{yr}, E_{xs}, and E_{ys} (the reference and sample data we are collecting), we obtain values for the Jones Matrix in terms of the data at each frequency. We assume that our material is isotropic, meaning the sample is independent of direction and there is no change as the sample is rotated by 90 degrees (i.e. $E_{xs}^{(1)} = E_{xs}^{(2)}$ and $E_{ys}^{(1)} = E_{ys}^{(2)}$ and therefore $t_{xx} = t_{yy}$ and $t_{xy} = -t_{yx}$), and the coefficients of the Jones matrix are described are as follows:

$$t_{xx} = t_{yy} = \frac{E_{xr}E_{xs} + E_{yr}E_{ys}}{E_{xr}^2 + E_{yr}^2} \tag{3.11}$$

$$t_{xy} = -t_{yx} = \frac{E_{yr}E_{xs} - E_{xr}E_{ys}}{E_{xr}^2 + E_{yr}^2} \tag{3.12}$$

As described in Section 2.1, we determine the TCD from the normalized difference between right and left circularly polarized fields

$$TCD = \tan^{-1}\left(\frac{E_R - E_L}{E_R + E_L}\right) \tag{3.13}$$

where

$$E_R = \sqrt{\left(\frac{\left|(t_{xx} + it_{yx})\right|^2 + \left|(t_{xy} + it_{yy})\right|^2}{2}\right)} \tag{3.14}$$

$$E_L = \sqrt{\left(\frac{\left|(t_{xx} - it_{yx})\right|^2 + \left|(t_{xy} - it_{yy})\right|^2}{2}\right)} \tag{3.15}$$

From this point, we simply perform these calculations on the fitted and transformed reference and sample data to calculate TCD for each sample at various frequencies. We find that using the substrate data as the reference data (rather than air) yields the most accurate results (see Chapter 4 for further explanation).

3.4 Calculation of Absorption

We use the relative absorption to decide which frequencies are of most interest. We use Eq. 3.16 to calculate the absorption. E_{xr} and E_{yr} correspond to the E_x and E_y components of the reference data. In our case, we used the substrate data as the reference data. E_{xs} and E_{ys} correspond to the E_x and E_y components of the sample data. In both cases, the E_x and E_y values are deduced from the model fit (see Section 3.2).

$$abs = \log_{10}\left(\frac{\left|E_{xr}^2 + E_{yr}^2\right|}{\left|E_{xs}^2 + E_{ys}^2\right|}\right) \tag{3.16}$$

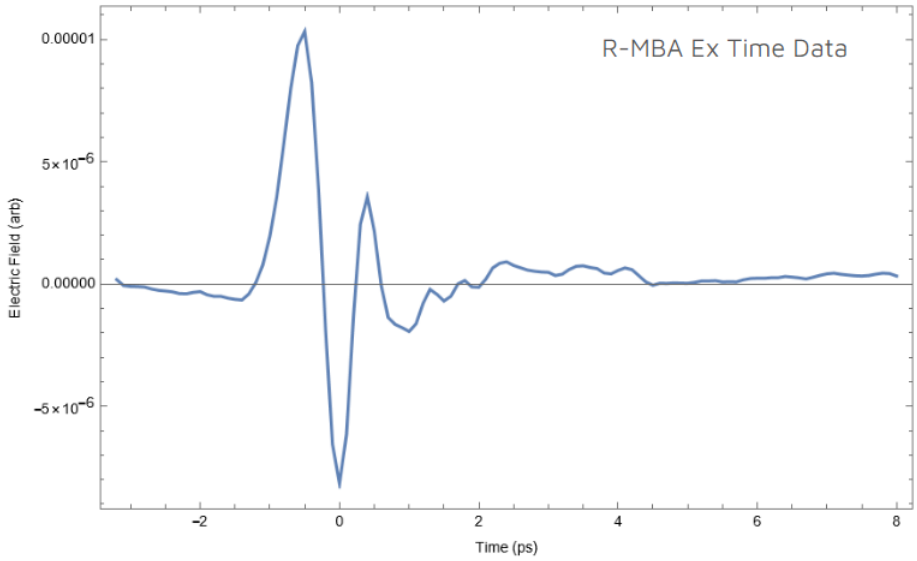

Figure 3.6 R-MBA_2PbI_4 E_x Time Data. This is the horizontal component of the field after passing through the sample before P2[2].

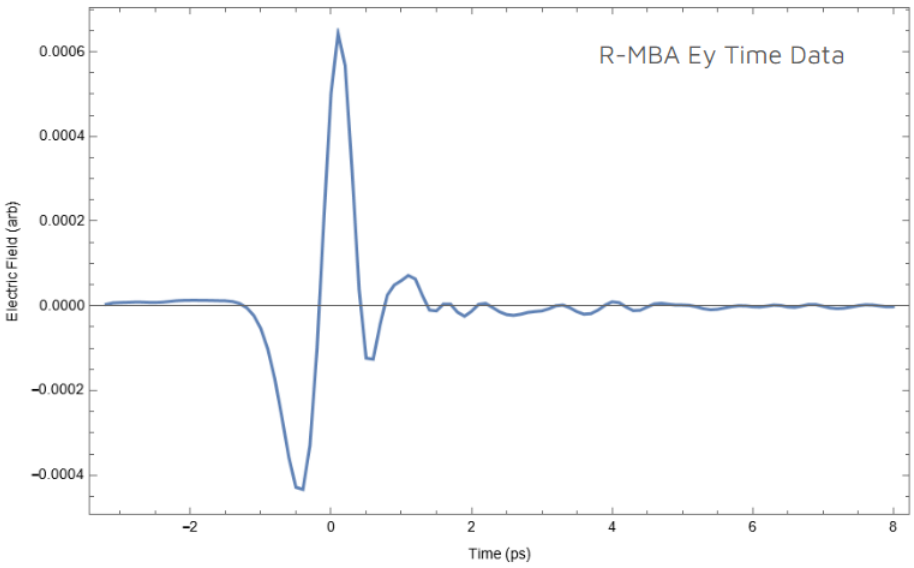

Figure 3.7 R-MBA_2PbI_4 E_y Time Data. This is the vertical component of the field after passing through the sample before P2.

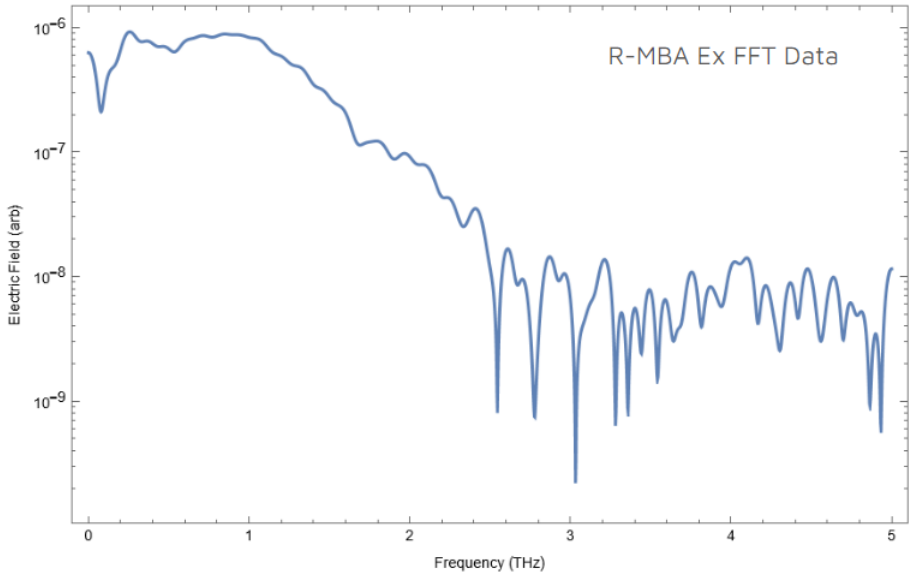

Figure 3.8 R-MBA_2PbI_4 E_x Frequency Data. This is the horizontal component of the field after passing through the sample before P2.

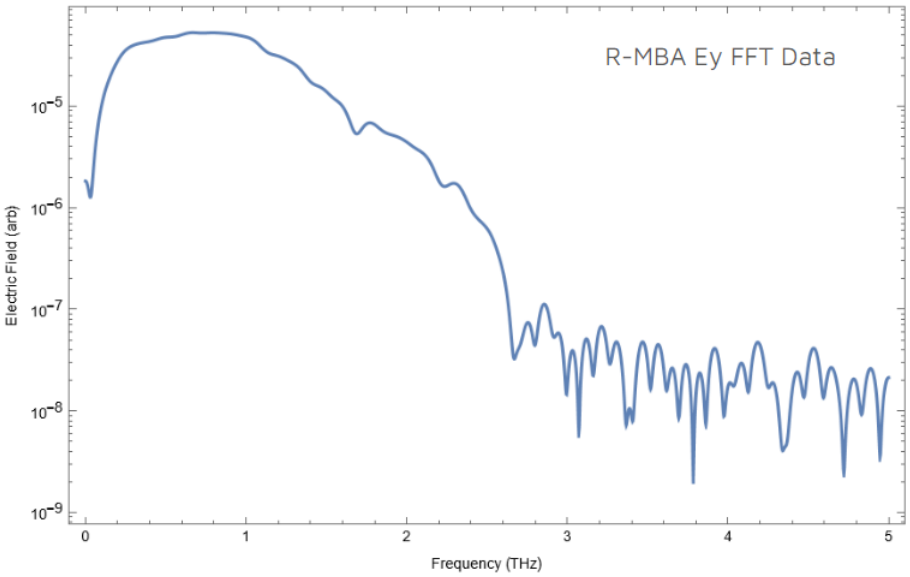

Figure 3.9 R-MBA_2PbI_4 E_y Frequency Data. This is the vertical component of the field after passing through the sample before P2.

Chapter 4

Results

Figures 4.1, 4.2, and 4.3 show the results from September 27, 2023. The substrate was five stacks of sapphire. The sample was five stacks of R-MBA_2PbI_4 on sapphire. The data was taken over a period of 11.2 ps labeled from -3.2 ps to 8 ps in intervals of 0.1 ps. This was done for 13 angles, ranging from 90 degrees to 90 degrees in 15-degree intervals.[1] Fig. 4.1 shows TCD (blue) and absorption data (red) versus frequency. For both TCD and absorption, the reference data used is the substrate data, rather than the air data. Fig. 4.2 shows the same data as Fig. 4.1, focusing on frequencies between 2.4 to 2.7 THz, where we suspect the most relevant information will be. Fig. 4.3 includes four plots showing TCD data for the different elements of the experiment. That is, sapphire TCD using air as the reference data, sample TCD using air as a reference, sample TCD using the sapphire as a reference, and finally a plot showing that the difference betweeen the sample TCD with air as a reference and the sample TCD with sapphire as a reference is approximately equal to the sapphire TCD versus air. This is expected and adds validity to our methods of data analysis.

[1] File Sep27_002, the air data includes 26 angles form 90 degrees to 35 degrees in 5-degree increments.

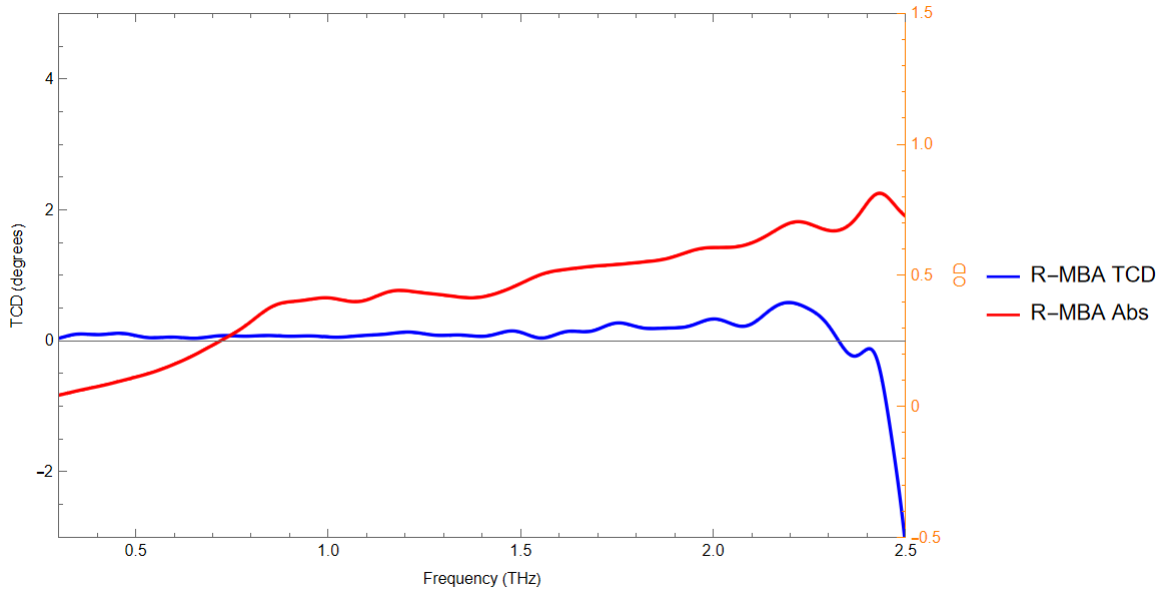

Figure 4.1 R-MBA_2PbI_4 TCD and Absorption. Data taken on September 27, 2023. Data plotted from 0.3 to 2.5 THz.

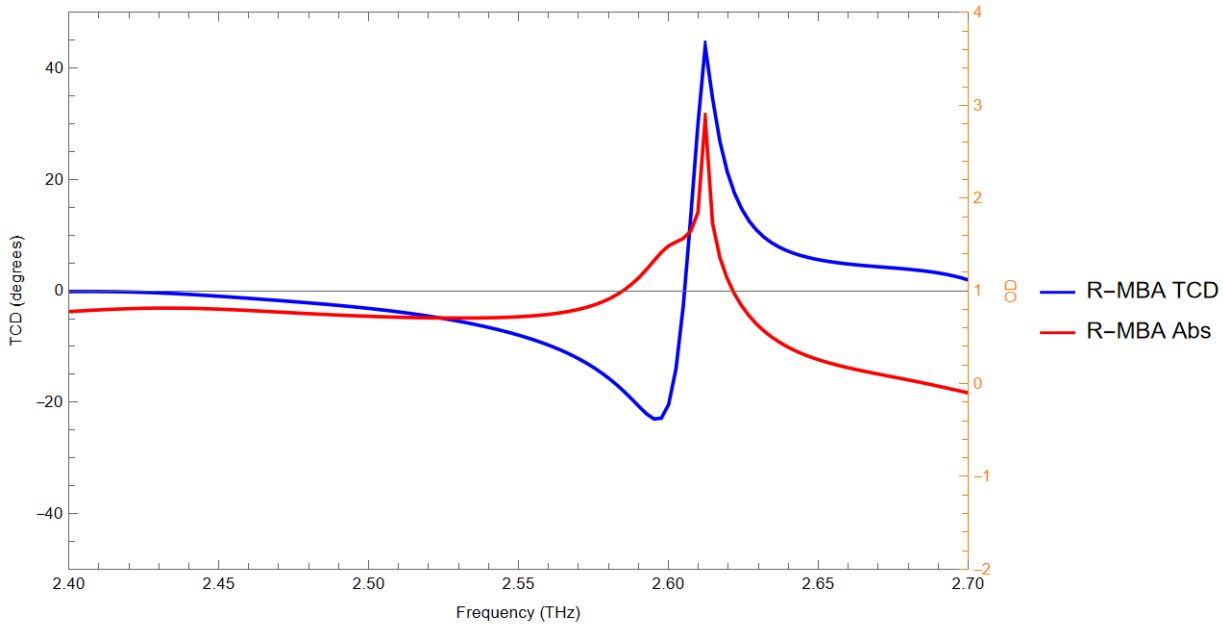

Figure 4.2 Zoomed in R-MBA_2PbI_4 TCD and Absorption. Data taken on September 27, 2023. Data plotted from 2.4 to 2.7 THz. Notice the TCD spike corresponds to the absorption spike.

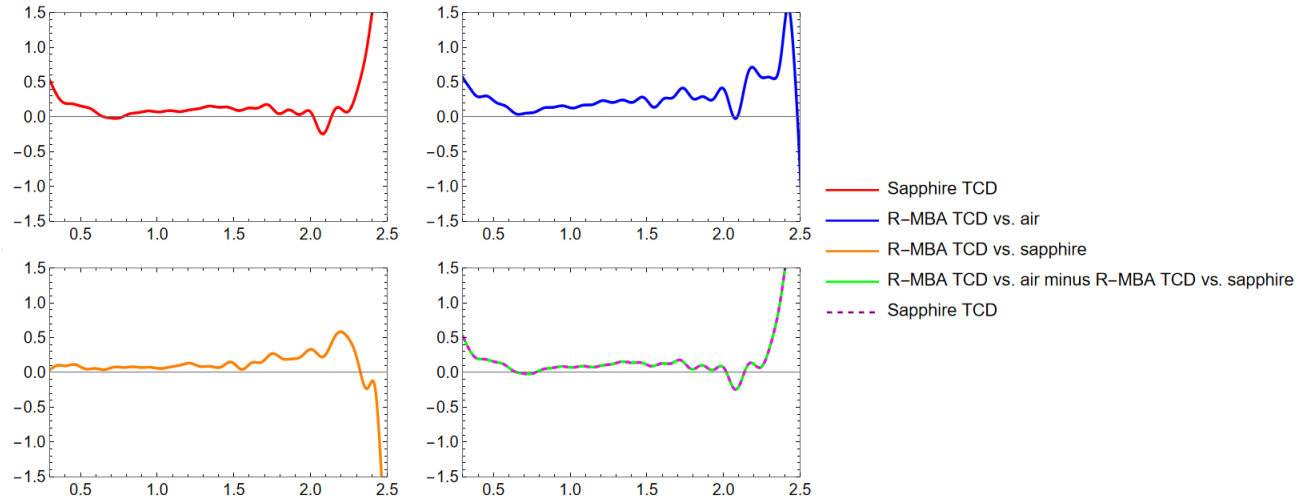

Figure 4.3 September 27, 2023 R-MBA$_2$PbI$_4$ TCD Summary. Sapphire TCD vs air (top left). R-MBA TCD vs air (top right). R-MBA TCD vs sapphire (bottom left). the bottom right corner shows two data sets: the green is sapphire TCD vs air, the purple dashed is the difference between the sample TCD vs air and the sample TCD vs sapphire.

Notice in Fig. 4.3 that the sapphire TCD is approximately equal to the difference between the sample TCD versus air and the sample TCD vs sapphire. This is reassuring as it suggests that the relationship between the sapphire TCD and the sample TCD is accurate. For this reason, we feel it is accurate to report the TCD of the sample using the substrate as a reference.

Figures 4.4, 4.5, 4.6, and 4.7 show the results from October 19th, 2023. The substrate was one stack of quartz. The samples were one stack of R-MBA$_2$PbI$_4$ on quartz and one stack of S-MBA$_2$PbI$_4$ on quartz. Each data set was taken over a period of 15 ps (-5 ps to 10 ps) in intervals of 0.1 ps. This was done for 9 angles, ranging from -60 degrees to 60 degrees in 15-degree intervals. Fig. 4.4 shows S-MBA TCD (blue) and absorption data (red) versus frequency. For both TCD and absorption, the reference data used is the substrate data, rather than the air data. Fig. 4.5 shows the same data as Fig. 4.4, focusing on frequencies between 2.4 to 2.7 THz, where we suspect the most relevant information will be. Figs. 4.6 and 4.7 include four plots each showing TCD data for the different elements of the experiment. That is, quartz TCD using air as the reference data,

sample TCD using air as a reference, sample TCD using the quartz as a reference, and finally a plot showing that the difference betweeen the sample TCD with air as a reference and the sample TCD with quartz as a reference is approximately equal to the quartz TCD versus air. This is expected and adds validity to our methods of data analysis.

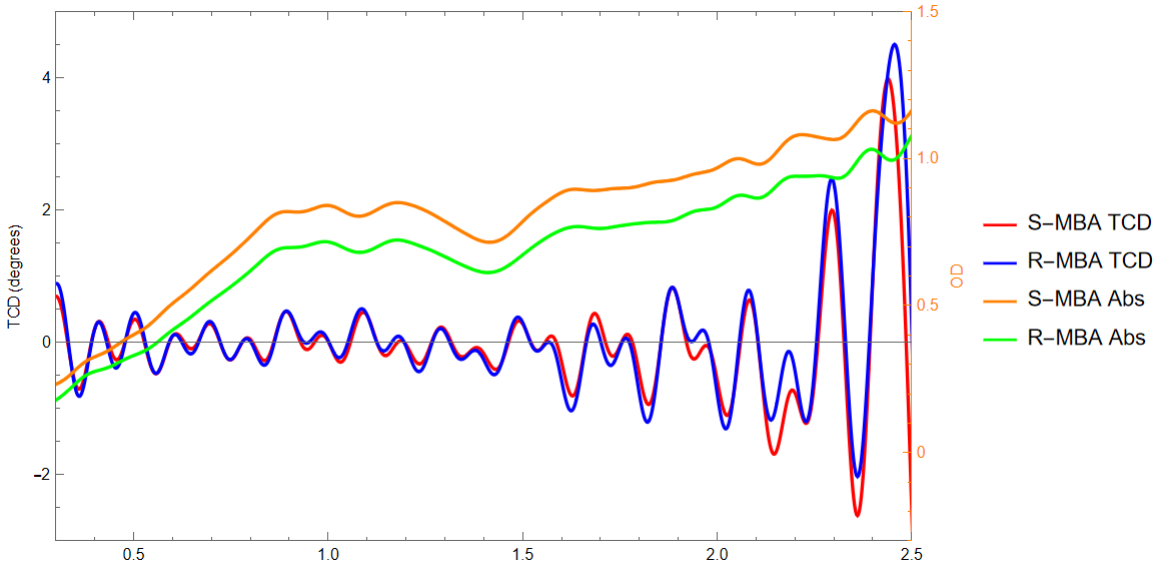

Figure 4.4 R-MBA_2PbI_4 and -MBA_2PbI_4 TCD and Absorption. Data taken on October 19, 2023. Data plotted from 0.3 to 2.5 THz.

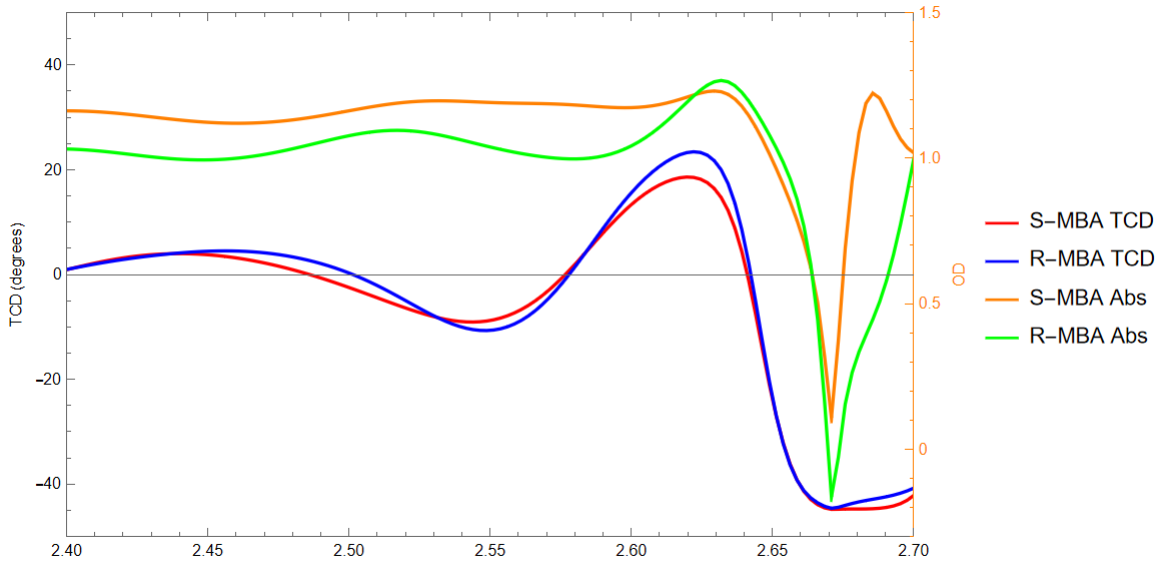

Figure 4.5 Zoomed in R-MBA_2PbI_4 and S-MBA_2PbI_4 TCD and Absorption. Data taken on October 19, 2023. Data plotted from 2.4 to 2.7 THz. Notice the TCD spike corresponds to the absorption spike.

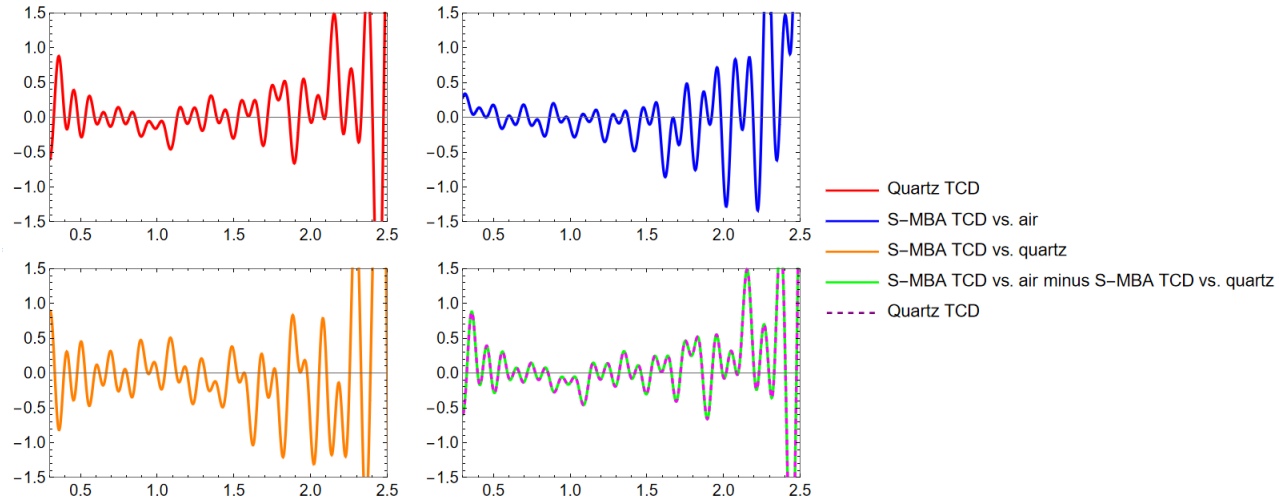

Figure 4.6 October 19, 2023 S-MBA_2PbI_4 TCD Summary. Quartz TCD vs air (top left). S-MBA TCD vs air (top right). S-MBA TCD vs quartz (bottom left). the bottom right corner shows two data sets: the green is quartz TCD vs air, the purple dashed is the difference between the sample TCD vs air and the sample TCD vs quartz.

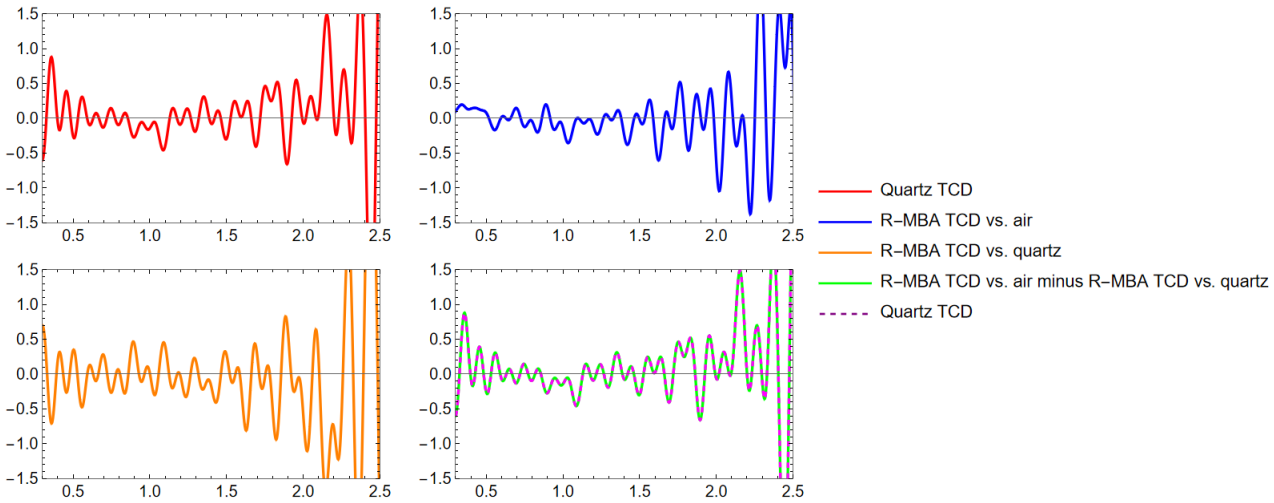

Figure 4.7 October 19, 2023 R-MBA$_2$PbI$_4$ TCD Summary. Quartz TCD vs air (top left). R-MBA TCD vs air (top right). R-MBA TCD vs quartz (bottom left). the bottom right corner shows two data sets: the green is quartz TCD vs air, the purple dashed is the difference between the sample TCD vs air and the sample TCD vs quartz.

Figures 4.8, 4.9, 4.10, and 4.11 show the results from May 31st, 2024. The substrate was one stack of quartz. The samples were one stack of R-MBA$_2$PbI$_4$ on quartz and one stack of S-MBA$_2$PbI$_4$ on quartz. Each data set was taken over a period of 11.2 ps (-3.2 to 8 ps in intervals of 0.1 ps).[2] Fig. 4.8 shows S-MBA TCD (blue) and absorption data (red) versus frequency. For both TCD and absorption, the reference data used is the substrate data, rather than the air data. Fig. 4.9 shows the same data as Fig. 4.8, focusing on frequencies between 2.4 to 2.7 THz, where we suspect the most relevant information will be. Figs. 4.10 and 4.11 include four plots each showing TCD data for the different elements of the experiment. That is, sapphire TCD using air as the reference data, sample TCD using air as a reference, sample TCD using the sapphire as a reference, and finally a plot showing that the difference betweeen the sample TCD with air as a reference and the sample TCD with sapphire as a reference is approximately equal to the sapphire TCD versus air. This is expected and adds validity to our methods of data analysis.

[2]File May30_002 contains air data with time intervals of 0.8 ps. Normally, the same separation is necessary to perform the calculations described in sec 3.3. In this case, adjustments were made to extrapolate data.

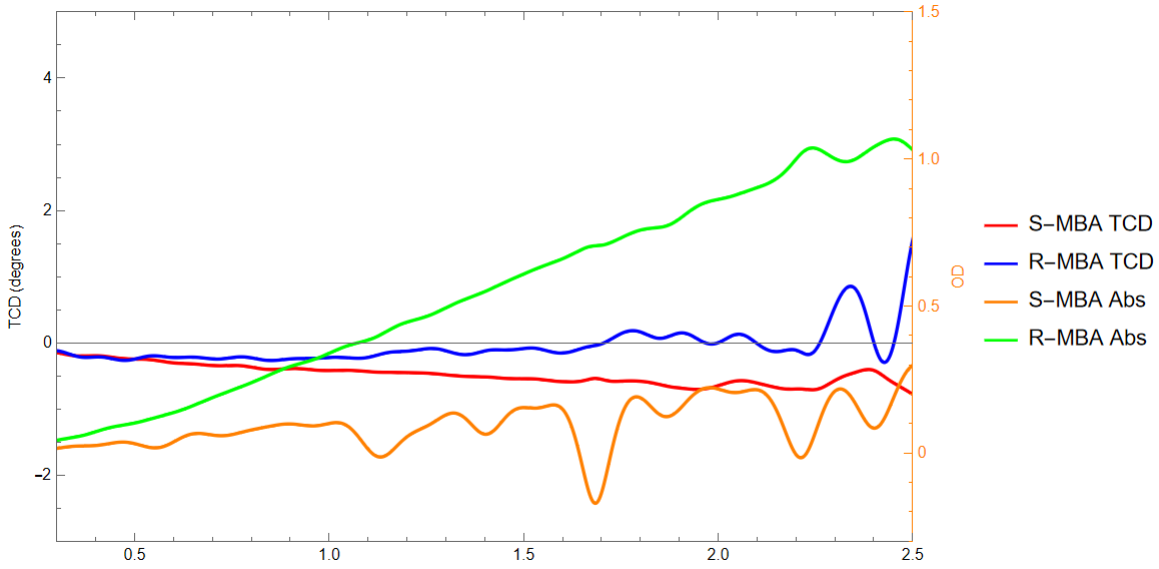

Figure 4.8 R-MBA_2PbI_4 and S-MBA_2PbI_4 TCD and Absorption. Data taken on May 31, 2024. Data plotted from 0.3 to 2.5 THz.

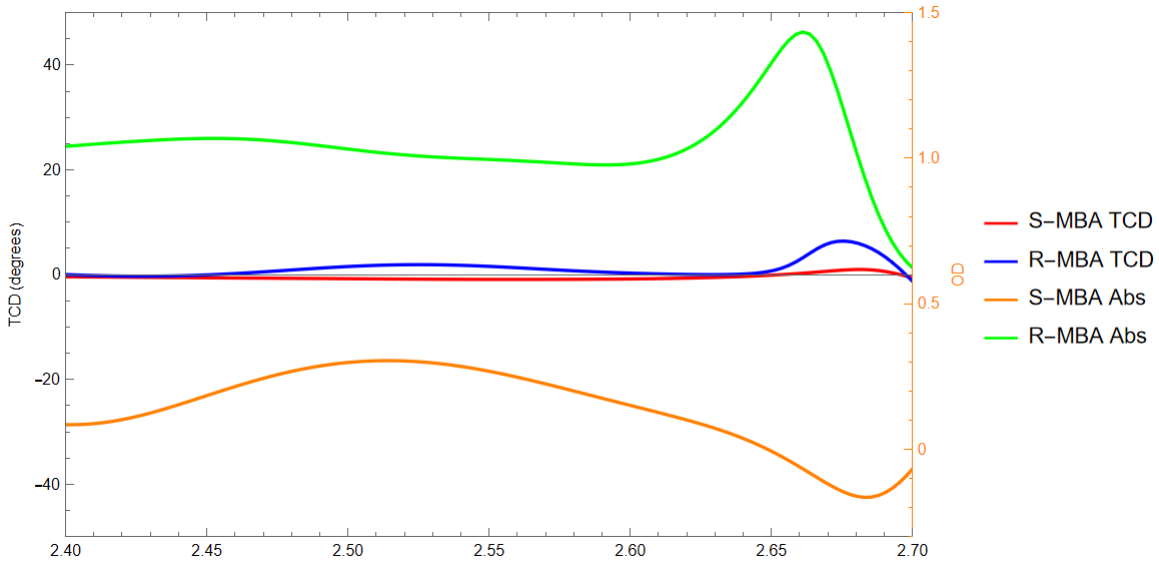

Figure 4.9 Zoomed in R-MBA_2PbI_4 and S-MBA_2PbI_4 TCD and Absorption. Data taken on May 31, 2024. Data plotted from 2.4 to 2.7 THz. Notice the TCD spike corresponds to the absorption spike.

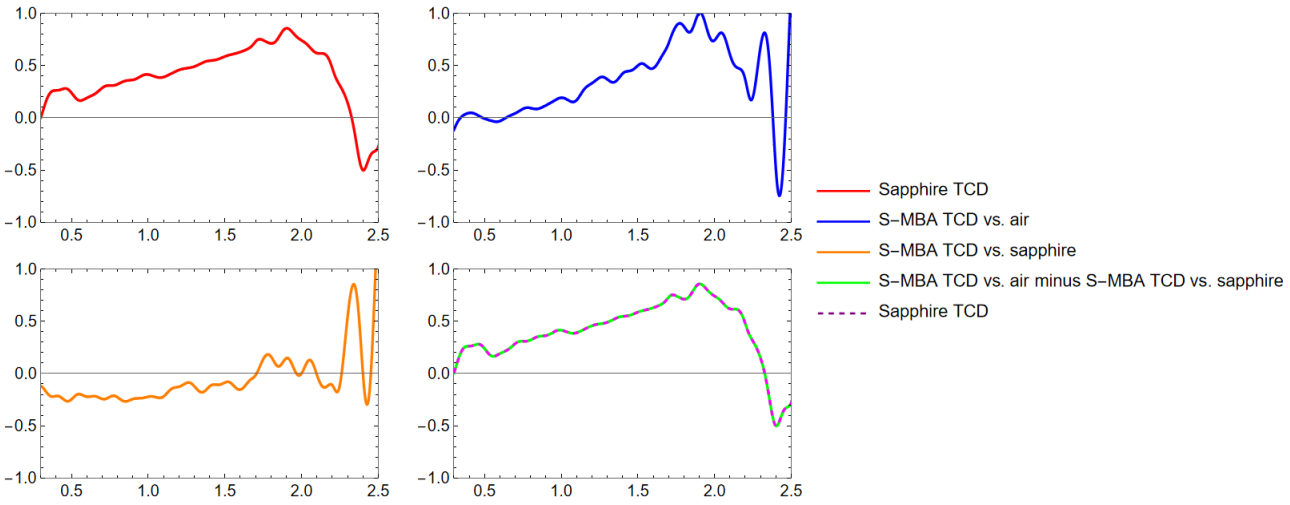

Figure 4.10 May 31, 2024 S-MBA_2PbI_4 TCD Summary. Sapphire TCD vs air (top left). S-MBA TCD vs air (top right). S-MBA TCD vs sapphire (bottom left). the bottom right corner shows two data sets: the green is sapphire TCD vs air, the purple dashed is the difference between the sample TCD vs air and the sample TCD vs sapphire.

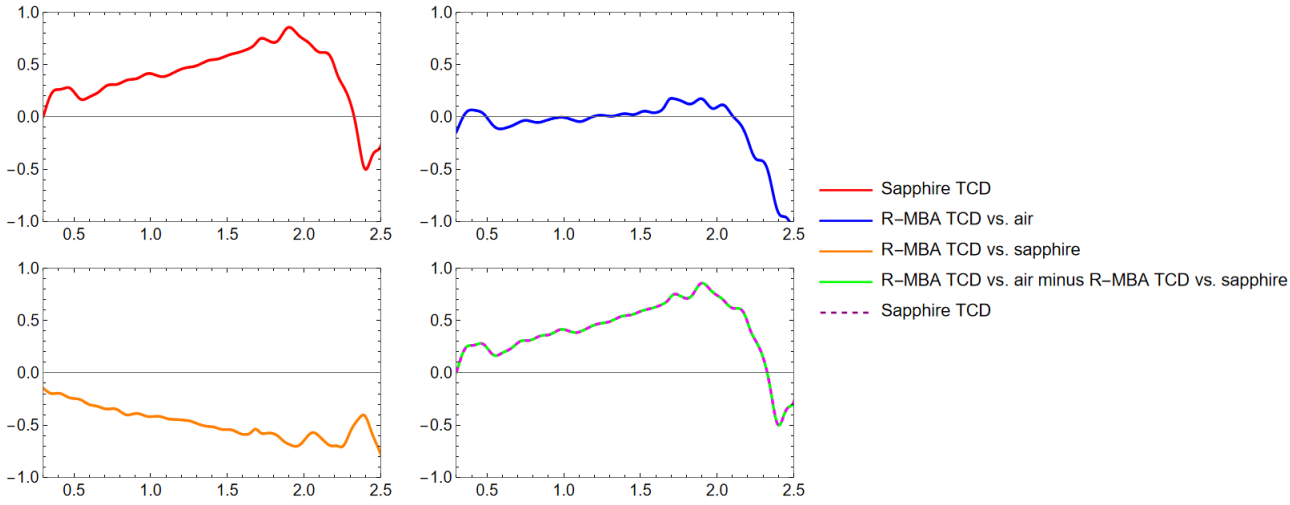

Figure 4.11 May 31, 2024 R-MBA_2PbI_4 TCD Summary. Sapphire TCD vs air (top left). R-MBA TCD vs air (top right). R-MBA TCD vs sapphire (bottom left). the bottom right corner shows two data sets: the green is sapphire TCD vs air, the purple dashed is the difference between the sample TCD vs air and the sample TCD vs sapphire.

Chapter 5

Conclusion

The data taken on September 27th includes only the R-enantiomer of MBA_2PbI_4. The sample was deposited on a sapphire substrate. Data was taken on five stacks of sample and substrate. The data shows a large absorption peak and a large TCD peak around 2.61 THz. We were unsure if this peak was a real physical feature, or if it was noise. Therefore, we hope to confirm the data with another experiment.

The data taken on October 19th includes both S- and R-MBA_2PbI_4. However, the substrate was quartz and data was taken on only one stack of sample and substrate. The data seems noisy. However, a closer look at frequencies between 2.4 to 2.7 THz shows R-MBA and S-MBA having very similar TCD signals, which is unexpected. Perhaps this has something to do with the substrate.

The data taken on May 31st includes both S- and R-MBA_2PbI_4. The substrate is sapphire. Each data set was taken on a stack of 5 samples and substrates. The data between 2.4 to 2.7 THz shows a similar trend to the data taken on October 19th, where the R-and S-enantiomers are very similar where we would expect them to be more opposite. Additionally, the absorption peak for R-MBA increases with frequency. We wonder, again, if the substrate's TCD signal is hiding that of the sample.

This project is still ongoing and will be continued by other students in John Colton's research group with our collaborators at NREL. Future data sets should include samples of R-MBA_2PbI_4 and S-MBA_2PbI_4 taken over a large period of angles. I would suggest -90 degrees to 90 degrees in 5 degree increments. We will expect to see that R-MBA and S-MBA hav approximately opposite TCD signals when referenced with the substrate data.

We especially will be interested to observe a phonon-related absorption peak that has an associated TCD peak at the same frequency. If we see such a feature, we will hope to confirm that trend with additional data sets.

It is possible that the sapphire substrates have a large TCD signal relative to the TCD of the sample. Therefore, it may be necessary to experiment with different substrates in order to get a good TCD signal with our sample. Additional tests using spiral substrates (which would have a large TCD signal) will confirm whether our methods are viable.

Overall, we feel optimistic about the method we are using to collect and analyze data, although the data we have collected thus far does not give us conclusive results about the TCD of R/S-MBA_2PbI_4.

Appendix A

MultiNonLinearModelFit Code

```
Options[MultiNonlinearModelFit] = {AccuracyGoal → Automatic, ConfidenceLevel → 19/20,
   EvaluationMonitor → None, Gradient → Automatic, MaxIterations → Automatic,
    Method → Automatic, PrecisionGoal → Automatic, StepMonitor → None, Tolerance → Automatic,
   VarianceEstimatorFunction → Automatic,
    Weights → Automatic, WorkingPrecision → Automatic, "DatasetIndexSymbol" → n̤
};(* == Join[Options[NonlinearModelFit], {"DatasetIndexSymbol" → n̤}] *)

MultiNonlinearModelFit[datasets_, form_, fitParams_, independents : Except[_List], opts : OptionsPattern[]] :=
    MultiNonlinearModelFit[datasets, form, fitParams, {independents}, opts];

MultiNonlinearModelFit[datasets_, form : Except[_?AssociationQ], fitParams_, independents_, opts : OptionsPattern[]] :=
    MultiNonlinearModelFit[datasets, <|"Expressions" → form, "Constraints" → True|>, fitParams, independents, opts];


    MultiNonlinearModelFit[
        datasets : {__?(MatrixQ[#1, NumericQ] &)},
        assoc : KeyValuePattern[{
            "Expressions" → expressions_,
            "Constraints" → constraints_
        }] /; AssociationQ[assoc],
        fitParams_List,
        independents_List,
        opts : OptionsPattern[]
    ] := Module[{
        fitfun, weights, grad,
        numSets = Length[datasets],
        precision = Precision @ datasets,
        augmentedData,
        indexSymbol = OptionValue["DatasetIndexSymbol"]
    },
        augmentedData = Join @@ MapIndexed[
            Join[ConstantArray[N[#2, precision], Length[#1]], #1, 2] &,
            datasets
        ];
        fitfun = With[{
            conditions = Flatten @ Map[
                {#, Indexed[expressions, #]} &,
                Range[numSets]
            ]
        },
            Switch @@ Prepend[conditions, Round[indexSymbol]]
        ];
           grad = Replace[
               OptionValue[Gradient],
               Automatic /; ListQ[expressions] :> D[fitfun, {Replace[fitParams, {v_, ___} :> v, {1}]}]
           ];
           weights = Replace[
               OptionValue[Weights],
               {
                   (list_List)?(VectorQ[#1, NumericQ] &) /; Length[list] === numSets :>
                       Join @@ MapThread[ConstantArray, {list, Length /@ datasets}],
                   list : {__?(VectorQ[#1, NumericQ] &)} /; Length /@ list === Length /@ datasets :>
                       Join @@ list,
                   "InverseLengthWeights" :> Join @@ Map[
                       ConstantArray[N[1 / #1, precision], #1] &,
                       Length /@ datasets
                   ]
               }
           ];
           NonlinearModelFit[
               augmentedData,
               If[TrueQ[constraints], fitfun, {fitfun, constraints}],
               fitParams,
               Flatten[{indexSymbol, independents}],
               Weights → weights,
               Gradient → grad,
               Sequence @@ FilterRules[{opts}, Options[NonlinearModelFit]]
           ]
       ];
```

Figure A.1 Mathematica Notebook. MultiNonLinearModelFit Code 2

Appendix B

Angle Offset Mathematica Code

Initialize matrix for the data

```
(*creating a three dimensional array for ease of manipulation*)
multiData = ConstantArray[0, {Length[timeList], Length[angleList], 2}];
numtimes = timeList // Length; (*store the number of time points for ease of iteration*)
```

Load the matrix with the data in the format we want

```
(*For every time point, create a dataset organized by angle, field magnitude*)
For[i = 1, i ≤ numtimes, i++,
  multiData[[i, All, 1]] = angleList;
  multiData[[i, All, 2]] = fieldData[[i]]
 ];
```

Create parameter List for MultiNonlinearModelFit

```
(*each point in time, no matter the angle, will be scaled by some field magnitude,
create an individual parameter for each point in time*)
indices = Range[1, numtimes];
"A" <> ToString[#] & /@ indices;
variables = ToExpression[%];
```

Figure B.1 Mathematica Notebook. Angle Offset Code 1

Testing with the MultiNonlinearModelFit

```
(*model to fit to, each dataset will share the same x0, but the amplitude will vary,
which is taken care of by the table*)
f = Table[variables[[i]] Sin[2 (x - x0) Degree], {i, 1, numtimes}];
params = AppendTo[variables[[1 ;; numtimes]], x0];
(*includes every amplitude and x0*)

fit = MultiNonlinearModelFit[multiData, f, params, x];(*perform the model fit, this step takes some time*)

x0best = x0 /. fit["BestFitParameters"];(*save x0, which is the angle offset we are interested in*)
```

Figure B.2 Mathematica Notebook. Angle Offset Code 2

Appendix C

E_x and E_y Mathematica Code

```
(*initialize and load matrix for data*)
airmultiData = ConstantArray[0, {Length[timeList], Length[angleList], 2}];
For[k = 1, k ≤ Length[timeList], k++,
  airmultiData[[k, All, 1]] = angleList;
  airmultiData[[k, All, 2]] = airIntensityData[[k]];
 ];

(*create model and parameters*)
f = Sin[x Degree] Cos[x Degree] Ey + Cos[x Degree]^2 Ex;
params = {{Ex, 0}, {Ey, 0.00001}};

(*perform fit and store values*)
airEyData = ConstantArray[0, Length[timeList]];
airExData = airEyData;

For[i = 1, i ≤ Length[timeList], i++,
 loopfit = NonlinearModelFit[airmultiData[[i]], f , params, x];
 airEyData[[i]] = {timeList[[i]], Ey /. loopfit["BestFitParameters"]};
 airExData[[i]] = {timeList[[i]], Ex /. loopfit["BestFitParameters"]};
]
```

Figure C.1 Mathematica Notebook. Code to fit E_x and E_y data.

Bibliography

[1] T. Wang, H. Sun, X. Li, and L. Zhang, "Chiral Phonons: Prediction, Verification, and Application," Nano Letters 24 (2024).

[2] Wikipedia, "Phonon," https://en.wikipedia.org/wiki/Phonon (Accessed May 29, 2024).

[3] H. Z. et al, "Observation of chiral phonons," American Association for the Advancement of Science **359,** 579–582 (2018).

[4] M. Abramowitz and M. W. Davidson, "Polarization of Light," https://www.olympus-lifescience.com/en/microscope-resource/primer/lightandcolor/polarization/ (Accessed May 7, 2024).

[5] H. Yao, E. Wynendaele, X.Xu, A. Kosgei, and B. Spiegeleer, "Circular dichroism in functional quality evaluation of medicines," J.Pharm.Biomed.Anal. 147 (2018).

[6] W. J. Choi, S. H. Lee, B. C. Park, and N. A. Kotov, "Terahertz Circular Dichroism Spectroscopy of Molecular Assemblies and Nanostructures," J. Am. Chem. Soc. **144,** 22789–22804 (2022).

[7] Wikipedia, "Molecular vibration," https://en.wikipedia.org/wiki/Molecular_vibration#:~:text=The%20typical%20vibrational%20frequencies%20range,approximately%2030%20to%203%20%CE%BCm. (Accessed May 28, 2024).

[8] Wikipedia, "Units of CD Measurment," https://www.chem.uci.edu/~dmitryf/manuals/Fundamentals/CD%20practical%20guide.pdf (Accessed June 5, 2024).

[9] N. Hurlburt, "Circular Dichroism," https://chem.libretexts.org/Bookshelves/Physical_and_Theoretical_Chemistry_Textbook_Maps/Supplemental_Modules_(Physical_and_Theoretical_Chemistry)/Spectroscopy/Electronic_Spectroscopy/Circular_Dichroism (Accessed May 9, 2024).

[10] G. Cheng, W. Choi, H. Jang, N. Kotov, and T. Norris, "Terahertz time-domain polarimetry for generalized anisotropic and chiral materials," Proc. SPIE 10917 (2019).

[11] Wikipedia, "Perovskite (structure)," https://en.wikipedia.org/wiki/Perovskite_(structure) (Accessed June 5, 2024).

[12] Q. A. Akkerman and L. Manna, "What defines a Halide Perovskite?," ACS Energy Letters 5 (2020).

[13] L. H, Z. V. Vardeny, and M. C. Beard, "Control of light, spin and charge with chiral metal halide semiconductors," Nature Reviews Chemistry **6,** 470–485 (2022).

[14] S. Apergi, G. Brocks, and S. Tao, "Calculating the Circular Dichroism of Chiral Halide Perovskites: A Tight-Binding Approach," J. Phys. Chem. Lett. **14,** 11565–11572 (2023).